Study On Thermal/Moisture Expansion Stress Of A Drop-Out Fuse Insulator

Jun Li, Suhui Zhang*, Jinpeng Xie, Fei Jiang, Zhaoyu Zhang, and Guangru Zhang

Electric Power Research Institute of State Grid Gansu Electric Power Company, Lanzhou, Gansu, 730070, China

** Corresponding author. E-mail: 1434081501@qq.com*

Received: October 15, 2024; Accepted: March 03, 2025

Drop-out fuses are widely used electrical devices, and their reliability directly affects the safety of power supply systems. Porcelain insulators, as a critical component, are prone to cracking, which significantly disrupts the order of power production. Therefore, starting from the perspective of stresses caused by mechanical external forces, environmental temperature changes, and moisture-induced expansion of cement adhesive, the stress distribution of porcelain insulators is analyzed to determine the causes of failure. The study reveals that the maximum stress induced by environmental temperature rise occurs at the contact interface between the adhesive hole in the middle of the insulator and the cement adhesive. When the temperature rises by 50 K, the porcelain insulator still maintains relatively good strength. However, the cement adhesive is subjected to significant shear stress, resulting in a failure zone near the adhesive hole. Consequently, the damage to the cement adhesive caused by temperature rise is identified as the primary reason for the failure of drop-out fuses. Additionally, the stress caused by moisture-induced expansion of the cement adhesive cannot be ignored. When the relative water absorption of the cement adhesive exceeds 90.3%, the compressive stress acting on it surpasses its allowable stress, leading to failure. Therefore, controlling the water absorption rate of the cement adhesive and delaying the ingress of moisture are critical measures to enhance the operational reliability of porcelain insulators.

Keywords: Fuse; Insulator; Thermal stress; Hygroscopic expansion

http://dx.doi.org/10.6180/jase.202601_29(1).0006

1. Introduction

Drop-out fuses serve as critical components on the high-voltage side of power supply lines within electrical grids and are widely used across the globe [1–3]. These fuses provide overcurrent protection and interrupting capabilities on the high-voltage side, characterized by their simple structure, clear breaking, and easy operation. They can be generally categorized into two types based on the material of the insulating parts: porcelain and rubber. Rubber materials are prone to aging in strong ultraviolet environments, while porcelain materials have better insulation performance [4] and thermal stability [5] compared to rubber materials. Therefore, drop-out fuses with porcelain insulators are more commonly used in the Northwest region of China.

The drop-out fuse primarily consists of a porcelain insulator, metal components, a fuse tube, and a fuse. During operation, the insulator provides support and insulation, featuring an umbrella-like structure on its exterior to increase the creepage distance. As shown in Fig. 1, the metal components serve as connectors and conductors. The current flows from the wire at the upper end of the insulator, through contacts, reaching the contact point at the top of the fuse tube, and then through the fuse inside the tube to the lower wire. When the current flowing through the fuse exceeds the rated value, the fuse will break, causing the top contact of the fuse tube to disconnect and drop down, thus

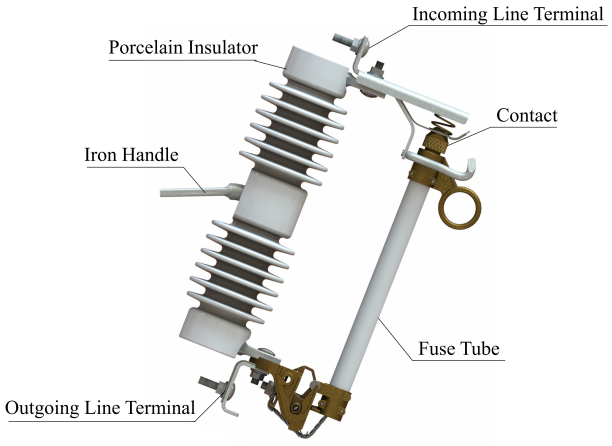

Fig. 1. Schematic diagram of a drop-out fuse.

interrupting the circuit.

Drop-out fuses have a wide range of applications, and power supply interruptions in the grid frequently occur due to faults in these fuses [6]. Due to its response time of only a few milliseconds, the drop-out fuse has an irreplaceable role in ensuring the safety of transformers [7]. The failure of porcelain insulators is the most common form of failure in drop-out fuses. Some insulators experience fractures during use due to adhesive and manufacturing defects [8], while others break due to uneven support installation [9]. During operation, faults in drop-out fuses often result in significant economic losses and considerable negative impacts. To address this issue, some researchers have designed specialized fault alarm devices for drop-out fuses, which can promptly identify the fault location. This facilitates the reduction of power outage duration [10].

The failure of drop-out fuses is primarily caused by the fracture of porcelain insulators. Porcelain insulators are subjected to gravity, wind loads, and the impact force generated during manual switching. In addition, the thermal stress on insulators caused by temperature fluctuations cannot be ignored. Sun's research indicates that the heating of porcelain induces crack propagation, leading to insulator fractures [11]. Wu identified that harsh climatic conditions are one of the main factors causing the rupture of post insulators [12]. Wang's study on the stress of post insulators under different temperatures revealed that significant stress exists at the interfaces of different materials within the insulator, and the cement adhesive is the weakest link in post insulators [13]. Zhang's research pointed out that temperature changes lead to stress concentration at the interface between the metal flange and the insulator, where the difference in materials' thermal expansion coefficients is the fundamental cause of the stress [14]. Liu highlighted that the structural strength of the metal components in post insulators has a significant safety margin, making such components generally less susceptible to failure [15]. These studies primarily analyze the potential causes of insulator fractures but lack an in-depth investigation into the stress distribution and failure mechanisms specific to the insulators of drop-out fuses. In particular, there is insufficient research into the fracture mechanisms of insulators under unique environmental and climatic conditions in Northwestern China, such as large temperature variations and strong wind events.

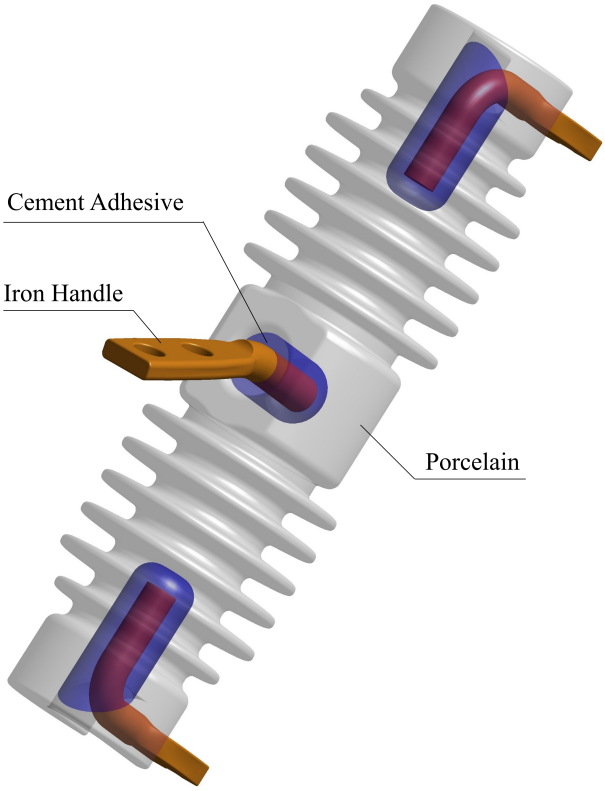

Fig. 2. Structures and geometric relationships of various materials in the insulator.

A porcelain insulator is mainly composed of three parts: metal components, cement adhesive, and an insulating porcelain body. Each component has different mechanical parameters and coefficients of thermal expansion due to differences in material. Fig. 2 shows the contact relationships among the insulator's components. The porcelain insulator is bonded to the metal components using cement adhesive, and the forces on the metal components are transmitted to the porcelain through this adhesive. Due to the differing thermal expansion coefficients of the three materials, internal stress can develop when the temperature changes. At the same time, the water absorption of cement adhesive

requires special attention during outdoor use [16]. The essence of cement adhesive is concrete, which readily absorbs moisture from the air in humid environments, such as during rainfall, resulting in a hydration reaction and subsequent expansion. This process generates hygroscopic expansion stress within the cement adhesive.

In humid environments or rainy weather, hydrophilic materials can exhibit hygroscopic expansion due to capillary absorption of water in the presence of internal voids [17]. Porcelain components are typically glazed, which prevents humid air from permeating them, and metallic parts are generally not susceptible to moisture absorption. However, cement adhesive readily absorbs moisture from the environment, leading to a hydration reaction and subsequent expansion [18]. This phenomenon significantly impacts the performance of porcelain insulators [19]. Hygroscopic expansion is a slow and continuous swelling process. For disk suspension insulators commonly used in high-voltage transmission lines, their hygroscopic expansion performance is typically verified through autoclave testing. According to the standards for disk suspension insulators, the expansion rate is required to be no greater than 0.1% [20]. However, there are no experimental requirements in the standards to test the hygroscopic expansion rate of the cement adhesive used in drop-out fuses, and its hygroscopic expansion is often overlooked. Studies have shown that the hygroscopic expansion rate of cement adhesive can reach up to 0.27% when it is unrestrained [18]. Therefore, it is necessary to investigate the stress state of cement adhesive in drop-out fuses after hygroscopic expansion.

In Northwestern China, the usage of porcelain insulators is substantial, and their maintenance costs are high. Existing research rarely addresses the impact of environmental temperature on the performance of drop-out fuse insulators, and the relevant standards for drop-out fuses have overlooked testing their hygroscopic expansion behavior. Considering the significant diurnal temperature variations and frequent strong winds in Northwestern China, the failure mechanisms of porcelain insulators in drop-out fuses become more complex. Therefore, it is necessary to investigate the environmental impacts on insulators, particularly the effects of temperature and humidity on the internal stress of insulators. This study examines thermal stress on insulators when subjected to an environmental temperature rise of 50 K and evaluates stress under varying relative humidity conditions. These findings are used to analyze the underlying mechanisms of insulator failure, providing guidance for the manufacturing and application of insulators.

2. Basic theories and numerical methods

This study establishes a geometric model of the RW-12kV dropout fuse and performs finite element analysis on the insulator component using the transient thermal module and structural static module in ANSYS software. During the analysis, it is assumed that the insulator is subjected to gravity, external loads, and temperature effects. The contact surfaces of various components of the insulator are assumed to remain bonded with no separation, the insulator is defect-free, the material is homogeneous and isotropic, and the deformation of the insulator is minor. Material parameters are derived from the literature and the material properties of porcelain, cement adhesive, and metal components are defined in the "engineering data" module in ANSYS. The reliability of the numerical method used in this study is validated by comparing the results with those from the literature. Boundary conditions for the insulator under actual operating conditions are set, and the effects of temperature and humidity on the internal stress of the insulator are analyzed.

2.1. Mathematical Model

For the thermoelastic mechanics problem studied in this paper, the stress and strain of the insulator are caused not only by external forces but also by temperature changes. Therefore, before conducting a structural mechanics analysis, the temperature distribution on the insulator should first be obtained. The structural strength is then analyzed under the combined effects of the temperature load and external load. The temperature variation of the insulator should satisfy the transient Fourier heat conduction law.

$$\rho c \frac{\partial T}{\partial t} = k \left(\frac{\partial^2 T}{\partial^2 x} + \frac{\partial^2 T}{\partial^2 y} + \frac{\partial^2 T}{\partial^2 z} \right) \tag{1}$$

In the above equation, ρ is the density, c is the specific heat capacity, k represents the thermal conductivity, T denotes the temperature at various points, and t is the time.

At any given point within an elastic body, the requirements of static equilibrium must be satisfied. The equilibrium equation can be expressed in the following form:

$$\begin{aligned} (\lambda + G)\frac{\partial e}{\partial x} + G\nabla^2 u - \beta \frac{\partial T}{\partial x} + f_x = 0 \\ (\lambda + G)\frac{\partial e}{\partial y} + G\nabla^2 v - \beta \frac{\partial T}{\partial y} + f_y = 0 \\ (\lambda + G)\frac{\partial e}{\partial z} + G\nabla^2 w - \beta \frac{\partial T}{\partial z} + f_z = 0 \end{aligned} \tag{2}$$

In the equation, e denotes the volumetric strain, u, v and w represent displacements in the x, y, and z directions, respectively. The term f refers to the body force acting

on the elastic body, λ is the Lame constant, β denotes the thermal stress coefficient, and G is the shear modulus [21].

The volumetric strain e is given by:

$$e = \frac{\partial u}{\partial x} + \frac{\partial v}{\partial y} + \frac{\partial w}{\partial z} \tag{3}$$

The expression for Lamé's constants is:

$$\lambda = \frac{Ev}{(1+v)(1-2v)} \tag{4}$$

In the above expression, E represents the elastic modulus, and v denotes Poisson's ratio. The relationship between the thermal stress coefficient β and the coefficient of thermal expansion a is given by:

$$\beta = \frac{\alpha E}{1-2v} \tag{5}$$

Hygroscopic expansion is typically measured through experimental methods that assess the amount of expansion and deformation. However, there is a lack of mature constitutive models for numerically simulating hygroscopic expansion. The simulation of the thermal expansion process can be easily achieved using finite element software. Since hygroscopic expansion and thermal expansion are two analogous processes, the method for simulating thermal expansion in finite element software can be used to simulate the hygroscopic expansion of cement adhesive. For example, Zeng et al. [22] utilized the similarities between heat conduction and pore fluid flow to simulate the hygroscopic expansion of expansive soils using the thermal stress module in finite element software. Fan [23] derived the necessary thermal expansion and conductivity coefficients for the thermal stress module based on experimental data on the hygroscopic expansion of expansive soils. This approach verified the feasibility of using thermal expansion modules to simulate hygroscopic expansion.

In the context of hygroscopic processes, the thermal expansion coefficient used in thermal simulations corresponds to the hygroscopic expansion coefficient, while the thermal conductivity corresponds to the permeability coefficient. For the cement adhesive used in porcelain insulators, due to its small volume and the slow hygroscopic process, it may take several hundred days to reach saturation. Therefore, it can be assumed that the degree of moisture absorption is uniform throughout the cement adhesive, allowing us to focus on the expansion stress under steady-state, uniform moisture absorption conditions. Based on the similarity between temperature fields and stress fields, the strain due to hygroscopic expansion can be expressed in the following form [24]:

$$\varepsilon_w = \beta\,(w - w_0) \tag{6}$$

In the given equations, ε_χ represents the strain rate after hygroscopic expansion, β is the hygroscopic expansion coefficient, w is the relative humidity, and w_0 is the initial relative humidity. When the initial relative humidity is 0 and the saturated relative humidity is 1, different levels of relative humidity correspond to varying amounts of expansion.

2.2. Material Parameters

The material of the embedded metal components in porcelain insulators is carbon structural steel, with a diameter of 18 mm. The coefficient of linear elastic expansion for the metal components is relatively larger compared to that of the porcelain, and being embedded, it induces internal stress upon thermal expansion. The porcelain body of the insulator is made of porcelain material, which provides excellent insulating properties. Porcelain have high hardness and good stability, but they are also notably brittle. They exhibit strong compressive strength but weaker tensile strength. Notably, porcelains lack plastic deformation, and when deformation reaches a certain level, brittle fracture occurs [25]. Porcelain materials are classified as brittle materials, and their analysis typically employs the maximum principal stress theory. The criterion used is whether the maximum tensile stress is less than the tensile strength of the material. The cement adhesive exhibits a higher linear elastic expansion coefficient compared to porcelain. On one hand, this allows for better adhesion between the cement and the inner wall surface of the porcelain insulator. On the other hand, it induces internal stress within the porcelain. The physical properties of the materials used for the insulator are shown in Table 1. In the structural static analysis module of the ANSYS software, three new materials—structural steel, porcelain, and cement adhesive—were created under the "Engineering Data" section, and their material parameters were entered according to the data in Table 1.

The cement adhesive is primarily composed of portland cement and aggregate, and also includes additives such as water-reducing agents and expanding agents. The cement and aggregates are mixed in a certain ratio to formulate a cement adhesive. The standard JB/T 4307-2004 "Cement Adhesives for Insulator Bonding" specifies the performance parameters of cement adhesives of different strength grades. The compressive strength of ordinary cement adhesive is 54 MPa, medium-strength cement adhesive is 64 MPa, and high-strength cement adhesive is 83.5 MPa [20]. Cement adhesives are classified as concrete, which exhibits relatively high compressive strength but possesses low flexural and shear strength. In this study, the

Table 1. Physical properties of materials used in insulators.

Name	Elastic Modulus (GPa)	Density (kg/m^3)	Coefficient of Thermal Expansion ($1/^\circ C$)	Poisson's Ratio	Thermal Conductivity Coefficient $W/(mK)$	Specific Heat Capacity $J/(kgK)$	Allowable strength (MPa)
Metal component	210	7850	12×10^{-6}	0.3	60.5	434	355
Porcelain	76	2400	5.0×10^{-6}	0.2	1.86	816	200
Cement Adhesive	31	2300	14×10^{-6}	0.215	0.8	780	

cement adhesive primarily withstands the pressure caused by thermal stresses. At the same time, under the constraint of the porcelain body, the cement adhesive tends to extrude out of the bonding hole under compression.

Additionally, it is subjected to tangential stress on the bonding surface. For the interface between new and old concrete or the bonding surfaces of concrete and other materials, the bonding strength is relatively low. It is often necessary to add special adhesives to improve the shear strength [26]. Regarding the porcelain insulator of the drop-out fuse, experimental results from the literature show that the shear bonding strength of the cement adhesive used for the insulator is approximately 2.425 MPa, which is significantly lower than its flexural strength and compressive strength [27]. When concrete is subjected to shear stress, it is considered to experience deformation or fracture failure if the maximum shear stress exceeds its shear strength. Therefore, the Mohr-Coulomb theory is employed to analyze the strength of the cement adhesive in this study. The shear strength of the material can be expressed by the following formula [28]:

$$\tau = c + \sigma \cdot \tan \varphi \tag{7}$$

where τ represents the shear stress, σ is the normal stress, c is the cohesion, and φ is the internal friction angle. Based on experimental data from the literature [27], for high-strength cement adhesives, c is 2.153 MPa , and φ is 43.8°.

2.3. Boundary Conditions and Numerical Methods

During operation, the central iron handle of the insulator is bolted to the cross arm, while both the incoming and outgoing ends of the insulator are connected to electrical wires. The loading conditions of the insulator are shown in Fig. 3. In the structural static mechanics module of ANSYS, constraints are applied based on the loading conditions of the insulator. The contact surface between the central iron handle of the insulator and the crossarm is subjected to a remote constraint, restricting all displacements and rotations except those caused by temperature changes. The entire insulator is subjected to the action of gravity G, which is perpendicular to and directed downward from the contact surface of the central iron handle. Spring forces F_k, acting along the axis of the porcelain insulator, are applied at both the upper and lower end iron handles, affecting the contact surfaces between the iron handles and the fuse tube base. During operation, the upper end iron handle is subjected to a pulling force F directed along the pulling direction. According to the production process provided by the manufacturer, the spring force F_k does not exceed 60 N, and the pulling force F does not exceed 160 N. There is no relative

sliding or separation on the contact surfaces of different materials; therefore, the contact relationship between the cement adhesive and the iron handle, as well as between the cement adhesive and the porcelain insulator, is defined as a fully bonded contact.

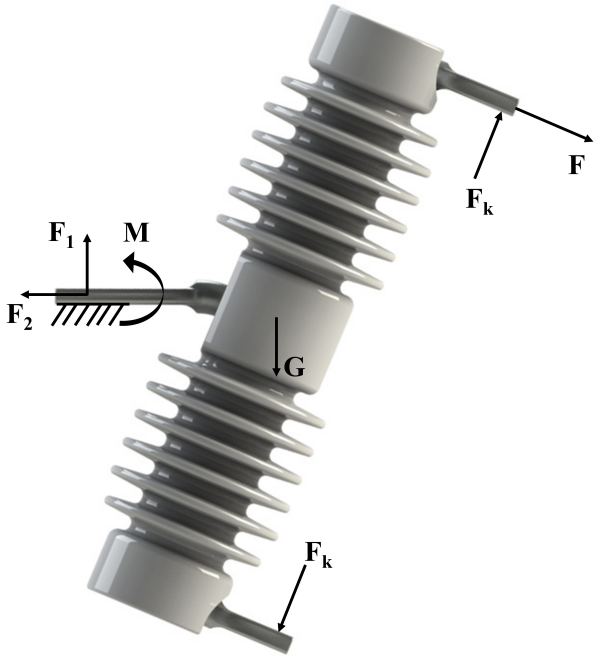

Fig. 3. Forces acting on the insulator.

When solving for the temperature field of the insulator, the transient thermal analysis module is used, where the initial temperature of the insulator is set to 20°C. A convective heat transfer coefficient $(100\ \mathrm{W/(m^2\ K)})$ is applied to all surfaces of the insulator exposed to air, and the incoming airflow temperature is set to the ambient temperature. This setup is designed to simulate the temperature variation of the insulator under strong wind conditions. Once the temperature field of the insulator is obtained, it is then imported into the structural static analysis module to solve for the resultant thermal stress.

The mesh module of ANSYS was utilized for meshing. The insulator of the drop-out fuse was modeled using SolidWorks software and imported into the geometry module of ANSYS. Predominantly tetrahedral and free triangular mesh structures are used. Mesh refinement was applied near the interfaces of the cement adhesive, metal components, and all different material boundaries. The total number of mesh elements was 2.14 million, and the mesh structure is shown in Fig. 4.

To validate the reliability of the numerical method used in this study, the same numerical method was applied to calculate the thermal stress on a post-type insulator in low-

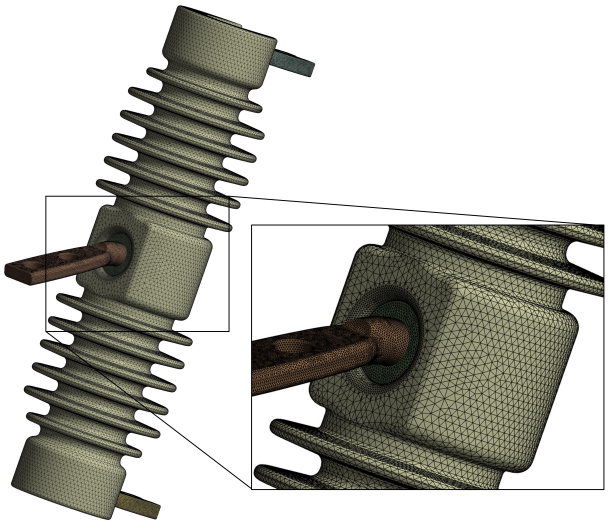

Fig. 4. The mesh of the insulator.

temperature environments as described in reference [29]. When the reference temperature is set to 18°C, the thermal stress on the post-type insulator increases as the temperature decreases. A comparison of the results obtained using the numerical method in this study with the results calculated using the formula provided in the reference is shown in Fig. 5. From Fig. 5, it can be observed that the results computed using the numerical method in this study are consistent with those in the reference, with an error margin of less than 5%. This indicates that the method employed in this study has good reliability in calculating thermal stress.

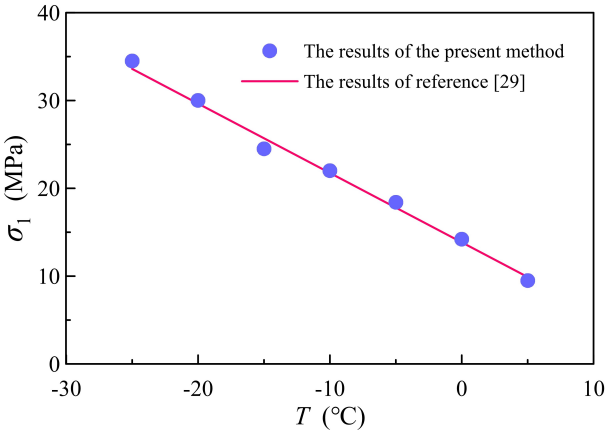

Fig. 5. Comparison of numerical results with results in the literature.

3. Results and discussion

During normal operation, the insulator is subjected to gravitational forces, spring forces, and tensile forces during operation. Under the influence of these mechanical forces, the maximum mechanical stress occurs at the bend in the middle iron handle of the insulator. When converted to Von Mises equivalent stress, it is approximately 278 MPa, which meets the strength requirements of the metal components and will not cause damage. Apart from the metal components, the maximum principal stress on the insulator is 7.78 MPa, located at the contact surface between the central iron handle and the cement adhesive. This indicates that stress is more concentrated at the joint of the central iron handle during operation of the fuse, but it is still less than the allowable stress of the cement adhesive. The maximum principal stress at the bonding site between the cement adhesive and the porcelain insulator is approximately 4.17 MPa. This stress is relatively low compared to the mechanical strength of the insulator, and no damage will occur at this part under normal operations.

3.1. Transient Thermal Stress during Environmental Temperature Changes

In the summer, many regions in China experience high temperatures, especially in areas such as Xinjiang, Gansu, and Xi'an, where local surface temperatures can exceed 70°C. When the ambient temperature is high, the sudden occurrence of strong winds or heavy rain causes the insulator to undergo a cooling process. Setting the initial temperature of the insulator at 70°C, with the convective heat transfer coefficient of the insulator and metal components surface being 100 W/ $(m^2\ K)$, and the incoming air temperature at 20°C, the insulator's temperature will rapidly decrease under such strong convection conditions. The varied temperature distribution across different areas causes different expansion rates, leading to internal stress within the insulator.

During the temperature drop process, the stress on the insulator decreases as the temperature drops. The stress on the insulator is at its maximum at the beginning of the cooling process. The distribution of the principal stress is shown in Fig. 6(a). The stress concentration occurs near the cemented holes in the middle of the insulator and at the root of the insulator shed. The maximum tensile stress is 44.35 MPa and occurs near the cemented hole of the porcelain insulator, while the maximum compressive stress is 20.24 MPa and appears on the cement adhesive within the cemented hole in the middle of the insulator. The deformation of the insulator is shown in Fig. 6(b). With the central iron handle fixed, the two ends of the insulator expand outward when heated, with a maximum displacement of 1.11 mm.

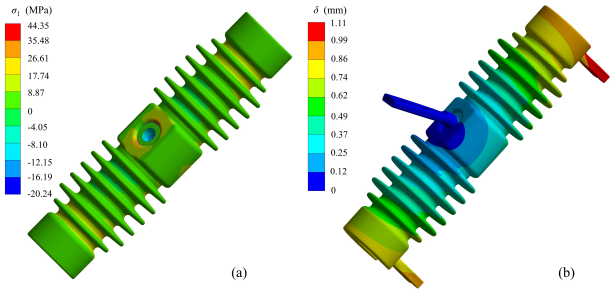

Fig. 6. The distribution of principal stress and deformation on the insulator.

The temperature variation of the insulator over time causes the stress on the insulator to change accordingly. The magnitude of the stress is related to the temperature gradient across different regions of the material. During the cooling process, the outer surface with a lower temperature contracts first, while the inner layer contracts later. As a result, the outer surface is subjected to tensile stress from the inner layer, which can be expressed as [30]:

$$\sigma_s = \frac{E\alpha\Delta T}{1-v} \tag{8}$$

In the equation, ΔT represents the temperature difference. For common porcelain, the elastic modulus is approximately 60 to 80 GPa , Poisson's ratio is 0.2 , and the coefficient of thermal expansion is $5.0 \times 10^{-6}/°C$. When the temperature of the porcelain rapidly changes from 70°C to 20°C, the possible maximum stress is 25 MPa . This result is generally consistent with the numerical simulation results, where the stress on the surface of the insulator is mostly below 26.61 MPa . Based on the above calculations and the simulation process, the insulator demonstrates adequate strength under sudden temperature changes and is not prone to failure after several temperature fluctuations. However, for fatigue failure of the insulator under cyclic thermal loads, further research is required using the fatigue life curve of the porcelain material.

When the operating temperature of an insulator exceeds the temperature of its production environment, thermal stress is generated internally. Figure 7 illustrates the variation curves of the insulator's average temperature and maximum principal stress over time, with an initial temperature of 20°C, a convective heat transfer coefficient of 100 W/ $(m^2\ K)$, and an incoming air temperature of 70°C. As shown in the figure, the average temperature of the insulator continuously rises over time, reaching equilibrium at approximately 1800 seconds. The magnitude of

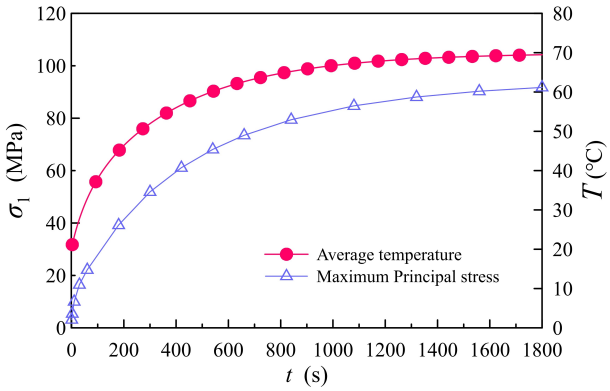

Fig. 7. Variation of average temperature and maximum principal stress of the insulator over time.

stress on the insulator is related to the temperature increase of the insulator; as the insulator's temperature rises, the maximum principal stress on the insulator also increases. The stress is mainly concentrated on the contact surface between the cement adhesive and the central cemented hole of the porcelain insulator, with a stress distribution similar to that in Fig. 6(a). The maximum tensile stress at the central cemented hole of the porcelain insulator is approximately 40.6 MPa . The maximum tensile stress experienced by the porcelain insulator is less than the allowable stress for porcelains, which is 200 MPa. Generally, the porcelain insulator will not fail due to operational forces and thermal stress, although the possibility of breakage cannot be excluded if there are internal defects, such as high porosity. The stress changes in the insulator during cooling and heating processes indicate that the maximum principal stress on the insulator is primarily related to the final temperature of the insulator, with a weaker relationship to time. Time affects the magnitude of thermal stress by influencing heat conduction. When the temperature tends to become uniform, the main factor determining the magnitude of thermal stress is the difference in thermal expansion coefficients of various materials, while the temperature gradient caused by differences in thermal conductivity has a smaller impact on thermal stress.

When the ambient temperature rises, the cement adhesive exhibits a larger expansion, causing it to tend to move outward from the bonding hole. At the contact surface between the cement adhesive and the bonding hole, the wall of the bonding hole constrains the outward displacement of the adhesive, resulting in shear stress on the cement adhesive directed inward by the wall surface. The contact surface within the cement joint is a weak point, as illustrated in Fig. 8(a). For different ambient temperatures, varying expansion rates result in tangential stresses of different magnitudes. Fig. 8(b) shows the relationship between the tangential stress on the two contact surfaces and the temperature increase. It can be observed that as the temperature rises, the tangential stress increases progressively. The tangential stress at the bonding interface between the cement adhesive and the porcelain body is significantly greater than that at the interface between the iron handle and the cement adhesive. At an ambient temperature increase of 50 K, the average tangential stress on the contact surface between the iron handle and the adhesive is 0.32 MPa, while the average tangential stress on the contact surface between the cement adhesive and the adhesive hole is 2.25 MPa. This tangential stress is below the shear strength at the bonding interface of the cement adhesive. The shear strength of the cement adhesive interface is approximately 2.425 MPa. When the tangential stress at the bonding interface between the porcelain body and the cement adhesive approaches the shear strength of the cement adhesive at a temperature increase of 50 K, the bonding interface becomes critical. Therefore, attention should be given to the tangential stress at the bonding interface between the cement adhesive and the porcelain body under temperature rise conditions to avoid potential failure caused by excessive temperature increases.

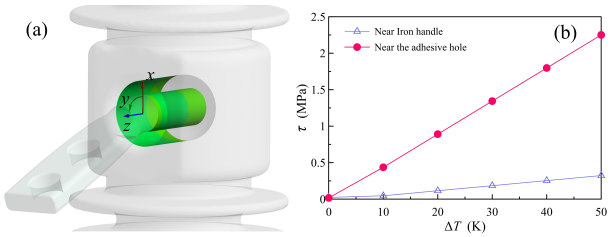

Fig. 8. Contact surface of cement adhesive and variation of tangential stress on the surface with temperature increase.

The safety of concrete is often analyzed using the Mohr-Coulomb theory, as the shear strength of concrete is significantly influenced by normal pressure. The Mohr-Coulomb theory effectively describes the shear performance and failure behavior of concrete. Based on the experimentally measured parameters c and φ of the cement adhesive from literature, the shear strength envelope of the cement adhesive is determined. Material failure occurs when the Mohr's circle is tangent to the shear strength envelope. In ANSYS, a safety factor f is used to evaluate the reliability of the material. Safety factor is defined as the ratio of the material's strength limit to the applied stress. When $f > 1$, the material is considered safe; when $f < 1$, the material fails. The distribution of the safety factor on the cement adhesive, based on the Mohr-Coulomb theory, is shown in Fig. 9. It

can be observed that when the ambient temperature rise is 50 K, the safety factor in areas near the adhesive hole is less than 1, indicating that the cement adhesive fails in these regions. This is largely consistent with the areas where similar insulators tend to fracture. The cement adhesive is also a weak point of the drop-out fuse insulator, and the shear stress exerted on the cement adhesive significantly impacts the reliability of the insulator.

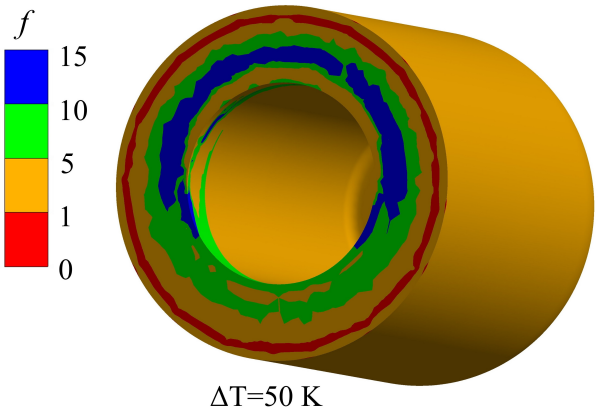

Fig. 9. Safety factor of the cement adhesive.

3.2. Stress Caused by Hygroscopic Expansion

For the cement adhesive, the expansion rate is 0.27% under saturated conditions. This leads to a calculation that yields an expansion coefficient $\beta = 0.0027$ at a 100% relative humidity. Therefore, the thermal-stress coupling module in ANSYS software can be employed to solve for the stress caused by hygroscopic expansion.

After moisture absorption, the distribution of maximum principal stress on the middle section of the cement adhesive in the insulator is shown in Fig. 10. Once the cement adhesive absorbs moisture and expands, it is constrained by the porcelain shell and subjected to compressive stress, with the maximum compressive stress reaching 92.48 MPa . At this stress level, even high-strength cement adhesive will be crushed. Fig. 11 shows the failure of the cement adhesive at the bonding hole in the middle of a drop-out fuse.

The outermost layer of the cement adhesive is squeezed out due to compression, reducing the bonding area between the metal handle and the porcelain shell. It can also be observed that the porcelain shell is subjected to tensile stress during the expansion of the cement adhesive, with the maximum tensile stress reaching 95.38 MPa. At this stress level, a high-quality porcelain insulator should not fracture. Therefore, once the cement adhesive becomes saturated with moisture, it will be extruded out from the

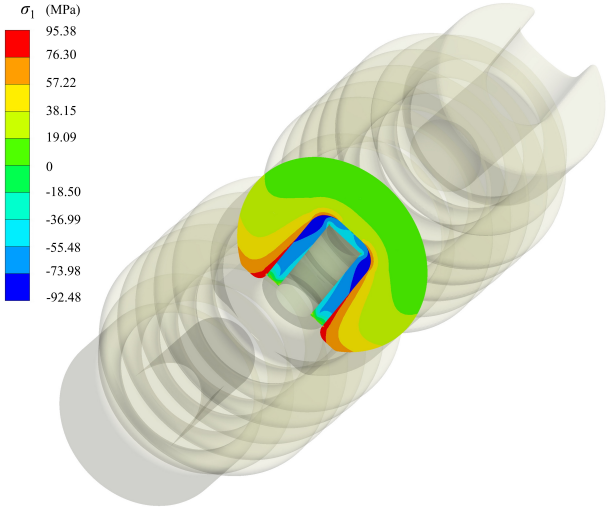

Fig. 10. Distribution of maximum principal stress in the middle section of the insulator during hygroscopic expansion.

Fig. 11. Failure diagram of cement adhesive in insulator.

bonding hole in the porcelain shell, causing the metal handle to detach from the bonding hole. Insulators that have not yet failed may eventually experience accidents due to rainwater intrusion and the corrosion-induced expansion of the metal handle in the future, ultimately leading to the fracture of the porcelain shell.

The hygroscopic expansion of cement adhesive is a slow-developing process, particularly for the cement in the bonding hole, where only the outer surface is exposed to air. Moisture gradually penetrates the interior of the cement through voids, leading to hydration reactions with minerals such as magnesium oxide, sulfates, and gypsum, which then cause expansion. The rate of water absorption directly influences the expansion rate of the cement adhesive.

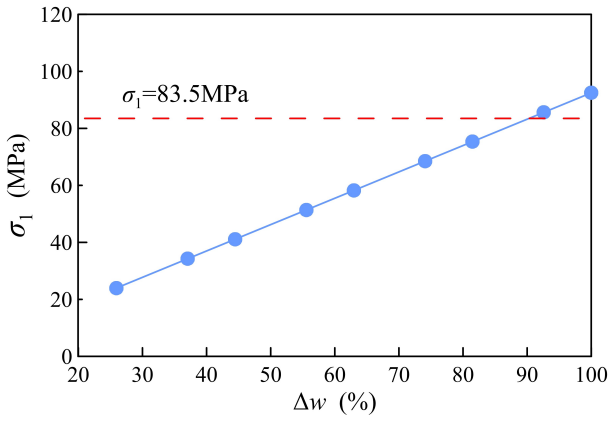

Fig. 12. Relationship between maximum principal stress and relative moisture content in the middle section of the insulator during hygroscopic expansion.

Different water absorption rates correspond to different expansion rates, leading to varying levels of stress. Fig. 12 illustrates the relationship between different moisture absorption rates and the maximum principal stress in the cement adhesive. The graph shows that the maximum principal stress increases with the increase in relative moisture content. When the relative moisture content reaches 90.3%, the maximum principal stress on the cement adhesive exceeds its allowable stress. Therefore, controlling the relative moisture content of the cement adhesive and slowing the ingress of moisture are crucial for enhancing the operational reliability of insulators. Applying waterproof coatings to the contact surface between the cement adhesive and air can reduce the moisture absorption rate, thereby extending its service life.

4. Conclusions

This paper examines the stress experienced by the insulator of a drop-out fuse under external mechanical loads, thermal loads, and the effects of hygroscopic expansion of cement adhesive. The study analyzes the impact of mechanical forces on the insulator when subjected to gravity, the spring force of the fuse tube, and operational pulling forces. The analysis considered the thermal stress caused by temperature variations between the curing environment and the actual operating environment of the insulator, as well as the stress induced by the hygroscopic expansion of the cement adhesive. The following conclusions were drawn from numerical simulations:

1. Under mechanical external forces, the maximum principal stress on the insulator is 7.78 MPa. This stress is lower than the allowable stress for both the porcelain body and the cement adhesive. Therefore, the current insulator will not experience failure under the effect of mechanical external forces alone.

2. When the ambient temperature rises by 50 K, the maximum principal stress reaches 40.6 MPa, occurring at the contact surface between the adhesive hole in the middle of the porcelain body and the cement adhesive. For a qualified porcelain body, this stress will not lead to failure. At this temperature increase, the tangential stress at the interface between the cement adhesive and the adhesive hole is 2.25 MPa, which is close to the shear strength of the cement adhesive bonding interface, 2.425 MPa. Using the Mohr-Coulomb theory to analyze the shear performance of the cement adhesive reveals that a failure zone exists near the adhesive hole in the cement adhesive. This indicates that the tangential stress caused by the temperature rise is the primary factor leading to the failure of the cement adhesive. Additionally, the maximum principal stress and tangential stress on the insulator depend on the maximum temperature rise of the insulator. This shows that the thermal stress on the insulator is primarily caused by the difference in thermal expansion coefficients of the materials, with a weaker correlation to the temperature gradient within the insulator.

3. When the relative moisture absorption rate of the cement adhesive reaches 90.3%, the compressive stress on the cement adhesive exceeds the allowable stress for high-strength cement adhesives. Consequently, the cause of insulator failure in drop-out fuses is the cracking of the cement adhesive after hygroscopic expansion. This allows rainwater to seep in, causing further freeze-thaw cycles and rust-induced expansion of metal components, ultimately resulting in the cracking of the insulator at the cemented hole. Therefore, it is essential to implement waterproofing measures for the cement adhesive used in insulators to delay or prevent moisture ingress, thereby enhancing their service life.

This paper analyzes the impact of environmental changes on the insulator, focusing only on its static strength under variations in temperature and humidity. However, it does not address wind loads during high winds or dynamic loads during operation. In particular, the fatigue strength of the insulator under cyclic wind loads requires further investigation.

5. Acknowledgment

The supporting of the State Grid Gansu Province Electric Power Company Major Project (No.52272223004M) is acknowledged.

References

[1] C. Lothongkam, T. Patcharoen, and S. Yoomak, (2023) *"Effect of the drop out fuse connection scheme on the overvoltage and the surge arrester in a distribution system"* **Energy Reports *9***: 41–47. DOI: 10.1016/j.egyr.2023.08.058.

[2] Q. Yang, X. Rong, R. Guo, H. Zhao, and Y. Zhao, (2022) *"Real-Time Detection of Insulators and Drop Fuses Based on Improved YOLOv4"* **Scientific Programming**: 5755265. DOI: 10.1155/2022/5755265.

[3] F. Wang, Q. Zhao, Y. Zhao, Z. Xu, H. Wu, T. Mu, H. Duan, and W. Yi, (2019) *"Analysis and Study on Material and Temperature Rise Test of 10kV Drop-Out Fuses"* **High Voltage Apparatus *55***(1): 80–86. DOI: 10.13296/j.1001-1609.hva.2019.01.013.

[4] B. Qi, Y. Zhang, X. Yang, Z. Yang, L. Lu, F. Yan, and C. Li, (2023) *"An Advanced Ceramic Material for Internal Insulation Used in Gas-Insulated HVDC Apparatus"* **IEEE Transactions on Dielectrics and Electrical Insulation *30***(2): 556–562. DOI: 10.1109/TDEI.2023.3247680.

[5] R. Gao, Z. Zhou, H. Zhang, X. Zhang, and Y. Wu, (2024) *"High-temperature service stability of a novel ceramic composite insulation material"* **Ceramics International *50***: 30402–30410. DOI: https://doi.org/10.1016/j.ceramint.2024.05.337.

[6] S. Wang, T. Chen, F. Teng, L. Liu, and X. Ren, (2021) *"Design of a Novel 12 kV Drop-Out Fuse Based on Shape Memory Alloy"* **High Voltage Apparatus *57***(10): 176–181. DOI: 10.13296/j.1001-1609.hva.2021.10.022.

[7] F. Wang, B. Li, W. Yi, Y. Zhao, and F. Lang, (2021) *"Operating Characteristics and Experimental Study of 12 kV Drop-out Fuse"* **Northeast Electric Power Technology *42***(8): 12–15.

[8] W. Guo, X. Chen, and S. Chen, (2020) *"Location Analysis and Prevention Strategies for a Breakdown Fault in a GIS Internal Busbar Support Insulator"* **Electric Porcelain and Arrester** (05): 248–253. DOI: 10.16188/j.isa.1003-8337.2020.05.041.

[9] Q. Sun, L. Wang, J. Fu, R. Zhang, Y. Zhou, and J. Zou, (2023) *"Study on Fracture Caused by Uneven End Face of Porcelain Insulator Support Platform"* **Electric Porcelain and Arrester** (3): 183–188. DOI: 10.16188/j.isa.1003-8337.2023.03.026.

[10] Z. Ju, W. Xing, W. Duan, H. Sun, X. Sun, and S. Liu, (2021) *"Research on Status Monitoring and Fault Alarm Device of Drop-out Fuse"* **Journal of Physics: Conference Series *1952***(3): 032084. DOI: 10.1088/1742-6596/1952/3/032084.

[11] Q. Sun, L. Wu, K. Lu, X. Liu, J. Jin, and D. Xu, (2023) *"Causes of Fractures in Suspension Porcelain Insulators"* **Physical & Chemical Inspection - Physics Section *59***(07): 61–63. DOI: 10.11973/lhjy-wl202307016.

[12] X. Wu and P. Wei, (2011) *"Failure Cause Analysis of a 220 kV Isolating Switch Porcelain Insulator"* **Electric Porcelain & Arresters** (06): 11–14+20. DOI: 10.16188/j.isa.1003-8337.2011.06.003.

[13] B. Wang, D. Zhang, Z. Yan, R. Yang, Q. Huang, B. Ma, and Z. He, (2020) *"Simulation Study on the Influence of Temperature on the Mechanical Properties of Porcelain Post Insulators"* **High Voltage Apparatus *56***(4): 74–79. DOI: 10.13296/j.1001-1609.hva.2020.04.012.

[14] E. Zhang, Y. Yang, W. Song, X. Wei, Z. Qiu, J. Ruan, and D. Huang, (2014) *"Thermal Stress Analysis of High Voltage Porcelain Post Insulator"* **Applied Mechanics & Materials *521***: 366–370. DOI: 10.4028/www.scientific.net/AMM.521.366.

[15] Z. Liu, W. Bi, X. Chen, J. Chen, D. Qi, and Y. Jiao, (2020) *"Structural Optimization Design of Metal Fittings for Porcelain Post Insulators"* **Electric Porcelain & Arresters** (04): 228–232. DOI: 10.16188/j.isa.1003-8337.2020.04.03.

[16] R. Yang, X. Kong, Z. Lu, Q. Wang, M. Zeng, and S. Zhou, (2017) *"Volume Deformation Performance and Mechanism of Cement Stone Under Water and Oil Absorption"* **Journal of the Chinese Ceramic Society *45***(2): 182–189. DOI: 10.14062/j.issn.0454-5648.2017.02.02.

[17] X. Ding, H. Zhao, and S. Huang, (2021) *"Study on Expansion Deformation Evolution Law of Rock Based on Hygroscopic–Expansion Analysis Model"* **Chinese Journal of Rock Mechanics and Engineering *40***(102): 3005–3013. DOI: 10.13722/j.cnki.jrme.2021.0603.

[18] Q. Wu, (1989) *"Mechanism of Expansion Failure in Cement Adhesive Used in Porcelain Suspension Insulators"* **Electric Porcelain and Arrester** (1): 34–42. DOI: 10.16188/j.isa.1003-8337.1989.01.007.

[19] P. Zhang, Y. Li, W. Wang, T. Ma, M. Cai, X. Yang, and D. Zhang, (2017) *"Cement-Based Adhesives for Electrical Porcelain and the Necessity of Standard Revision"* **Electric Porcelain and Arrester** (6): 177–180, 186. DOI: 10.16188/j.isa.1003-8337.2017.06.032.

[20] *JB/T4307 - 2004 Cement Adhesive for Insulator Assembly*. Xi'an Electric Porcelain Research Institute. China: China Standards Press, 2007.

[21] H. Chen, J. Zhang, D. Cong, M. Zhang, K. Song, Z. Li, and L. Xie, (2022) *"Finite Element Simulation of Temperature Field and Residual Stress for Tungsten Coating by Electric Spark Deposition"* **Surface Technology *51***(1): 140–149. DOI: 10.16490/j.cnki.issn.1001-3660.2022.01.015.

[22] Z. Zeng, B. Xu, S. Hu, and C. Chen, (2014) *"Numerical Analysis of Expansive Soil Tunnel Lining Failure Under Moistening Conditions"* **Rock and Soil Mechanics *35***(3): 871–880. DOI: 10.16285/j.rsm.2014.03.045.

[23] C. Fan, (2017) *"Numerical Simulation Study on Hygroscopic Expansion Characteristics of Expansive Soil in Hefei"* **Geotechnical Engineering *31***(6): 753–757.

[24] J. Yang, W. Zhao, and W. Zhao, (2018) *"Numerical Analysis of Tunnels in Expansive Surrounding Rock with Different Water Contents"* **Science & Technology Innovation and Application** (10): 1–4, 7. DOI: 10.19981/j.cn23-1581/g3.2018.10.001.

[25] Y. Lang, J. Zhao, C. Wang, and B. Liu, (2014) *"Fracture Behavior of Porous Ceramics with Medium Porosity Under Compression"* **Journal of the Chinese Ceramic Society** (12): 1528–1536.

[26] Q. Li, X. Yin, K. Guo, and S. Xu, (2022) *"Experimental Study on the Interfacial Shear Strength Between Ultra-High Toughness Cementitious Composites and Reactive Powder Concrete"* **Engineering Mechanics *39***(8): 232–244.

[27] S. Xu. *"Research on Mechanical Deformation Characteristics of Disc Suspension Insulators in Extremely Cold Regions"*. (mathesis). Hubei University of Technology, 2019.

[28] S. M. A. Hu Fang, S. M. A. Bozhong Lin, and M. A. Yao Yao, (2024) *"Mechanical Properties of the Interface between Reactive Powder Concrete and Aggregates at Different Temperatures"* **Journal of Engineering Mechanics *150***(12): 04024086. DOI: 10.1061/JENMDT.EMENG-7510.

[29] M. Chen, (2018) *"Analysis of Mechanical Properties and Critical Crack Size of Porcelain Post Insulators in Low-Temperature Environments"* **Electric Porcelain and Arrester** (4): 217–222. DOI: 10.16188/j.isa.1003-8337.2018.04.038.

[30] Y. Zhou. *Ceramic Materials Science*. Harbin Institute of Technology Press, 1995.